Int J Earth Sci (Geol Rundsch) (2011) 100:289–304
DOI 10.1007/s00531-010-0623-1

ORIGINAL PAPER

The basement of the Punta del Este Terrane (Uruguay): an African Mesoproterozoic fragment at the eastern border of the South American Río de La Plata craton

Miguel A. S. Basei · Elena Peel · Leda Sánchez Bettucci · Fernando Preciozzi · Allen P. Nutman

Received: 13 December 2009 / Accepted: 7 November 2010 / Published online: 30 November 2010

Abstract The Punta del Este Terrane (eastern Uruguay) lies in a complex Neoproterozoic (Brasiliano/Pan-African) orogenic zone considered to contain a suture between South American terranes to the west of Major Gercino–Sierra Ballena Suture Zone and eastern African affinities terranes. Zircon cores from Punta del Este Terrane basement orthogneisses have U–Pb ages of ca. 1,000 Ma, which indicate an lineage with the Namaqua Belt in Southwestern Africa. U–Pb zircon ages also provide the following information on the Punta del Este terrane: the orthogneisses containing the ca. 1,000 Ma inheritance formed at ca. 750 Ma; in contrast to the related terranes now in Africa, reworking of the Punta del Este Terrane during Brasiliano/Pan-African orogenesis was very intense, reaching granulite facies at ca. 640 Ma. The termination of the Brasiliano/Pan-African orogeny is marked by formation of acid volcanic and volcanoclastic rocks at ca. 570 Ma (Sierra de Aguirre Formation), formation of late sedimentary basins (San Carlos Formation) and then intrusion at ca. 535 Ma of post-tectonic granitoids (Santa Teresa and José Ignacio batholiths). The Punta del Este Terrane and unrelated western terranes represented by the Dom Feliciano Belt and the Río de La Plata Craton were in their present positions by ca. 535 Ma.

Keywords Mesoproterozoic · Punta del Este Terrane · Uruguay · Brasiliano orogeny · Gariep belt · U–Pb zircon ages

M. A. S. Basei · E. Peel
Instituto de Geociências, Universidade de São Paulo, São Paulo, Brazil

E. Peel · L. Sánchez Bettucci (✉)
Departamento de Geología, Instituto de Geología y Paleontología, Facultad de Ciencias, Universidad de la República Oriental del Uruguay, Iguá 4225, Malvin Norte, 11400 Montevideo, Uruguay
e-mail: leda@fcien.edu.uy

F. Preciozzi
Dirección Nacional de Minería y Geología, Hervidero 2861, Montevideo, Uruguay

A. P. Nutman
School of Earth and Environmental Sciences, University of Wollongong, Wollongong, NSW 2522, Australia

A. P. Nutman
Research School of Earth Sciences, Australian National University, Canberra, ACT 0200, Australia

Introduction

The Neoproterozoic belts that occur on both sides of the southern Atlantic Ocean reflect collisional orogeny between the Congo/São Francisco, Paranapanema, Río de La Plata and Kalahari cratons during the building of the Western Gondwana. In southwestern Africa, these belts correspond to the Kaoko, Damara, Gariep and Saldania belts, whereas the Ribeira, Dom Feliciano and Rocha belts represent their South American equivalents (Fig. 1a). The latter is considered to be the direct continuity of the Gariep belt (Basei et al. 2005).

Despite considerable amounts of new geological information, notably from South America, there are still considerable differences in opinion concerning the crustal architecture and sequence of events related to this orogeny that formed Western Gondwana. An important issue is whether there are relicts of oceanic crust present and the polarity of possible subduction zones. The generation of a 700–600 Ma magmatic arc resulting from westward-

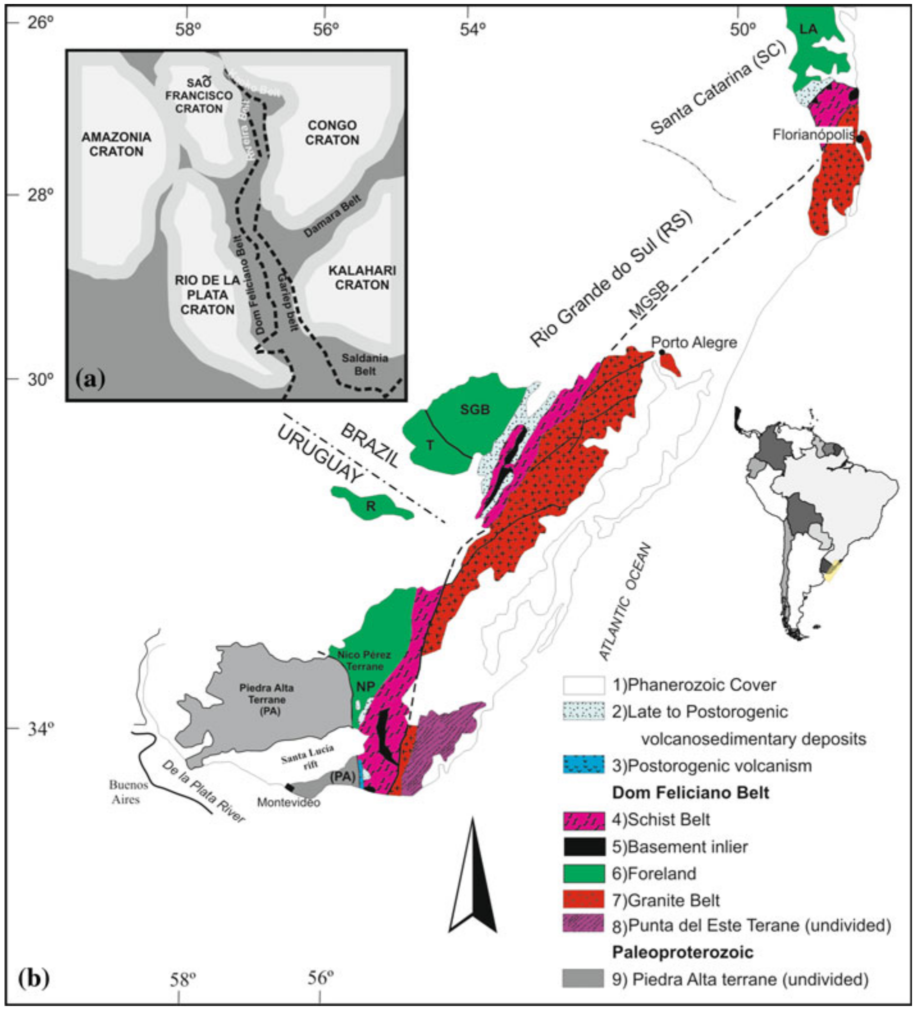

Fig. 1 **a** Paleogeographic outline showing the arrangement of major orogenic belts and cratons. **b** Geological sketch of Southern Brazil and Uruguay. *1* Phanerozoic covers undivided *2* Foreland basins: Itajaí (Santa Catarina State), Camaquã (RS), El Soldado-Piriápolis (UY) *3* Post-collisional volcanism *4* Schist belts and intrusive granitoids: Brusque metamorphic complex (SC), Porongos Metamorphic Complex (RS), Lavalleja Metamorphic Complex (UY) *5* Paleoproterozoic basement inliers: Morro do Boi (SC), Encantadas (RS) and Punta Rasa (UY) *6* Foreland: Luis Alves microplate (LA), Piedra Alta Terrane (PA), São Gabriel Block (SGB), Taquarembó (T), Rivera (R) and Nico Perez (NP) *7* Granite Belt: Florianópolis (SC), Pelotas (RS) and Aiguá (UY) batholiths *8* Punta del Este Terrane (PET) *9* Piedra Alta terrane (PA)

dipping subduction was suggested by Porada (1979), Fragoso Cesar (1991) and Chemale (2000). For the same time period, Ramos (1988) and Basei et al. (2000, 2005 and 2008) proposed east-dipping subduction, toward the Kalahari Craton. More recently, Oyhantçabal et al. (2009), Gaucher et al. 2009a, b) and Sánchez Bettucci et al. 2010a have suggested variations in westward-dipping subduction models.

The Punta del Este Terrane (PET) is interpreted as an exotic domain, tectonically juxtaposed to the Dom Feliciano Belt. It is composed of a gneissic-migmatitic basement covered by metasedimentary rocks of the Rocha Formation correlated with the western units of the Gariep belt in Namibia and South Africa (Basei et al. 2005). Considering the lack of a 1.2–1.0 Ga geological record in the southeastern portion of South America, the demonstration of any geological record of this age is fundamental to aid the positioning late Neoproterozoic sutures in paleogeographic reconstructions of Rodinia (Cordani et al. 2003, Tohver et al. 2006, Fuck et al. 2008, Li et al. 2008).

Therefore, the main objective of this work is to present new zircon U–Pb (SHRIMP and IDTIMS) and whole-rock Nd and Sr isotopic data for the gneissic-migmatitic rocks of the PET basement. These data, via the documentation of a Mesoproterozoic geological record, indicate that the PET basement units of Cerro Olivo Complex can be correlated with the Namaqua Belt of southwestern Africa. The correlation of supracrustal belts of both domains (Rocha and Gariep belts) has already been indicated by Basei et al. (2005).

Geological setting

The Neoproterozoic mobile belts found in southern Brazil and eastern Uruguay can be regarded as marking the limit of the Kalahari–Kapvaal and Congo cratons, now on the eastern side of the Atlantic in southwestern Africa. These mobile belts have several branches. The Damara belt within Africa separates the Congo and Kalahari cratons, and the Kaoko, Gariep and Saldania belts (from north to

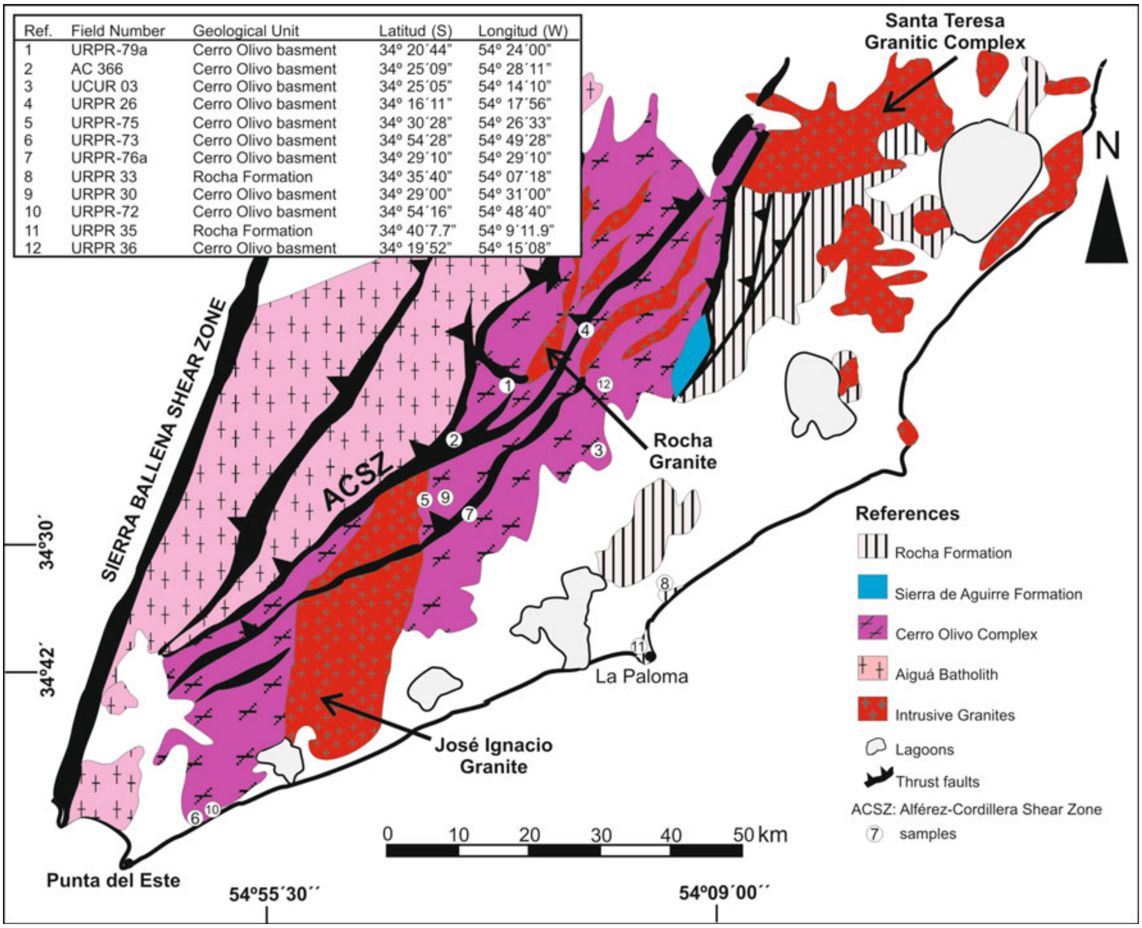

Fig. 2 Geological sketch of the Punta del Este terrane (simplified from Masquelin 1990)

south, respectively) occur along the coast of Africa. The Gariep belt and its basement are the most important geological units for comparison with the PET (Fig. 1b). The basement of the Gariep belt consists mostly of 1,200–1,100 Ma medium–high-grade metamorphic rocks (Clifford et al. 1981, Frimmel 1995) with some Paleoproterozoic basement inliers (Tack et al. 2002).

Regional correlations of the Mesoproterozoic belts of southern and central Africa have conventionally referred to them as Kibarian (Mesoproterozoic, Thomas et al. 1994). Based on geochronological and isotopic data, Eglington (2006) placed the Namaqua-Natal metamorphic climax at 1,200–1,040 Ma, with juvenile crust formation occurring at ca. 2,200 and 1,400 Ma. SHRIMP U–Pb zircon dating (Robb et al. 1998) indicated two crust-forming events in the Namaqua Complex at 1,220–1,170 Ma (Kibarian) and 1,060–1,030 Ma (Namaqualand). The Namaqua Metamorphic Complex is interpreted as a deformed and metamorphosed sedimentary passive margin succession at the west of the Kalahari craton (Becker et al. 2006; McCourt et al. 2006; among others). Related to the Kibarian event, there was regional deformation with granulite facies metamorphism and intrusion of granitoids represented by the Nababeep and Modderfontein gneisses. Based on geophysical data, the crustal thickness varies across the Namaqua front at the southwestern margin of the Kaapvaal craton and is linked to orogenic thickening at ca. 1,100–1,000 Ma (Schmitz and Bowring 2004 and references therein). These rocks are cut by the Concordia and Rietberg granitoids. The Pan-African tectonothermal overprint is not intense but is strongest in the west along the coastal region.

The Gariep belt occurs along the African coastal region and structurally overlies the Namaqua Metamorphic Complex. It is characterized by supracrustal rocks affected by very low to low metamorphic grade which are distributed into two tectono-stratigraphic domains. The eastern portion is marked by parautochthonous units related to a passive continental margin (Port Nolloth Zone) and the western portion by an allochthonous domain (Marmora Terrane). Suggestions of blueschist-facies metamorphism (Kröner 1974; Porada 1979) have been ruled out by Frimmel and Hartnady (1992); thus, these rocks are not regarded to have experienced (transient) high-pressure metamorphism. Gariep belt sedimentation occurred in the

Fig. 3 **a** Sillimanite-garnet-biotite paragneiss, URPR-73, Manantiales beach (–34°54′42.52″, −54°49′35.322″) **b** Rhythmic metasedimentary rocks, Rocha Formation, La Paloma beach (34°40′6.58″,−54°9′9.33″) **c** Deformed conglomerate with granite and volcanic clasts, San Carlos Formation (−34°50′28.35″, −54°53′24.93″) **d** AC-301, high evolved peraluminous granite, Bori Fernandes farm (−34°20′55.666″, −54°23′53.924″) **e** URPR-74 mafic granulite, Riet Correa farm (−34°23′28.42″, −54°14′32.29″) **f** Mylonites from the Alférez-Cordillera Shear Zone (−34°15′17.69″, −54°37′58.64″)

Neoproterozoic, based on 735 Ma ages for rhyolites of the Ross Pinah Formation (U–Pb single zircon evaporation technique; Frimmel 1995). Basei et al. (2005) demonstrated that the sediments of the Rocha Formation (supracrustal rocks of the PET) in Uruguay and the Gariep belt in southern Africa have a similar zircon age provenance pattern and suggested that they were probably deposited in the same basin. Unmetamorphosed sediments of the Nama Group cover the northeastern portion of the Gariep belt.

The most conspicuous feature, the Gariep belt, is the absence of any syn-tectonic calc-alkaline magmatism, suggesting it does not contain a volcanic arc. Granites considered to have formed in a pre-rift tectonic setting prior to formation of the Gariep rocks yielded Pb–Pb zircon ages of 830, 800 and 771 Ma (Frimmel et al. 2001). The youngest age is taken as the maximum age of sedimentation in the Gariep paleobasin. Evidence for syn-rift magmatism is given by two volcanic units, the ca. 750 Ma Rosh Pinah Formation and the older Vredefontein Formation (Frimmel et al. 2001). A deformational episode at ca. 545 Ma is related to the closure of the Adamastor Ocean between the Kalahari and the Río de La Plata cratons (Basei et al. 2000). Post-orogenic alkali granites and syenites (for example the 507 Ma Kuboos pluton) cut the central part of the Gariep belt along the Kuboos-Bremen line, which strikes SW-NE (Frimmel 2000).

In south Brazil and Uruguay, an old (pre-Mesoproterozoic) western domain known as the Río de La Plata Craton occurs (Fig. 1b). This craton includes the Piedra Alta and Nico Pérez tectonostratigraphic terranes that are separated by the Sarandí del Yí Shear Zone (Bossi and Campal 1992, Bossi et al. 1999, Rapela et al. 2007, Mallmann et al. 2007, Sánchez Bettucci et al. 2010a, b, Oyhantçabal et al. 2010a). The difference between these terranes is that the Piedra

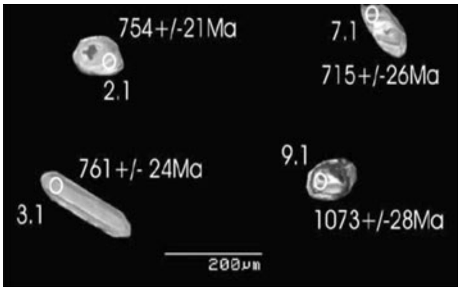

Fig. 4 Cathodoluminescence images of sectioned zircons from sample UCUR-03

Alta Terrane was not reworked in Neoproterozoic times, preserving its juvenile Paleoproterozoic character (Preciozzi et al. 1999; Bossi and Cingolani 2009; Sánchez Bettucci et al. 2010b, Oyhantçabal et al. 2010a). To the east, the Brasiliano/Pan-African orogenic cycle is represented in Uruguay and southern Brazil by the Dom Feliciano belt (DFB). In Uruguay, the DFB shows three petrotectonic domains: (a) western post-orogenic sequences, (b) the central supracrustal Lavalleja Group and Carapé Complex, and (c) to the eastern side of Sierra Ballena, the granitoids of Aiguá–Pelotas Batholith formed in a magmatic arc. The Lavalleja Group (Preciozzi et al. 1979, 1985; Bossi and Navarro 1988, Cingolani et al. 1990; Sánchez Bettucci et al. 2001, 2010a is located between the Nico Pérez Terrane and Sierra Ballena shear zone. It represents a meta-volcanosedimentary unit with some gneissic-migmatitic basement inliers and is cut by the Carapé Granitic Complex (Sánchez Bettucci et al. 2003, see Fig. 1). The Lavalleja Group is correlated with the Porongos and Brusque Groups in Brazil. To the east occurs the PET, separated from the Aiguá–Pelotas Batholith by the Alférez-Cordillera shear zone (Preciozzi et al. 1999, Basei et al. 2000).

Brasiliano post-orogenic magmatism climax at ca. 580 Ma and was closely related to transcurrent movements (e.g. the Major Gercino-Sierra Ballena and Alférez-Cordillera shear zones; Bitencourt and Nardi 2000; Koester et al. 2001, Oyhantçabal et al. 2005, 2009, 2010b, c; Florisbal et al. 2009; among others).

Punta del Este terrane (PET)

The PET (Preciozzi et al. 1999) only occurs in eastern Uruguay, between Punta del Este (south) and Velázquez (north). Its western limit with the Aiguá–Pelotas Batholith is defined by the Alférez-Cordillera lineament, which is an important shear zone consisting of a broad muscovite-bearing mylonite belt (Fig. 2). Granitoids of subalkaline affinity (Masquelin 1990) are emplaced along this lineament. The mylonitic foliation strikes between N15°and 40°E with steep NW to subvertical dips. Stretching lineations dip 20°–30° southwestward, and the kinematic indicators suggest a predominantly dextral oblique movement. This point to a reverse component, placing the Aiguá batholith above the PET rocks. The PET basement consists of variably deformed high-grade metamorphic rocks. Lithologies are gneisses, granite-gneisses, granulites and migmatites with intercalated calc-silicate rocks, amphibolites and quartzites (Preciozzi et al. 1999; Masquelin et al. 2001, Gross et al. 2009).

Table 1 U-Pb SHRIMP analytical data

Labels	U (ppm)	Th (ppm)	Th/U	Pb* (ppm)	^{204}Pb (ppb)	^{238}U/^{206}Pb	^{207}Pb/^{206}Pb	^{206}Pb/^{238}U		
								Age	Error	% Concor.
UCUR-1.1	404.3	71.6	0.177	46	10	8.45627	0.06617	720.51	56.19	88.8
UCUR-2.1	208.3	45.1	0.216	25	5	8.06436	0.06351	753.56	20.62	103.9
UCUR-3.1	237.1	43.8	0.185	29	0	7.98602	0.06561	760.53	23.92	95.8
UCUR-4.1	267.3	42.8	0.160	32	4	7.88312	0.06461	769.89	23.53	101.1
UCUR-7.1	108.1	32.3	0.299	13	2	8.52458	0.05965	715.05	26.40	89.4
UCUR-8.1	297.5	197.0	0.662	40	0	8.01075	0.06327	758.32	25.81	90.6
UCUR-10.1	293.9	34.1	0.116	32	15	8.27161	0.06511	735.72	20.37	121
UCUR-11.1	313.1	51.2	0.163	37	4	7.75712	0.06540	781.67	24.17	105.7
UCUR-12.1	169.7	97.0	0.572	34	6	7.98556	0.06553	760.57	21.82	90.6
UCUR-13.1	321.8	64.1	0.199	38	4	8.00240	0.06552	759.06	21.63	94.6
UCUR-15.1	280.9	44.6	0.159	35	1	8.12278	0.06565	748.44	36.99	99.3
UCUR-5.1	332.3	56.3	0.169	40	4	8.09052	0.06710	751.26	27.09	96.1
UCUR-6.1	297.3	45.8	0.154	36	3	8.18887	0.06643	742.74	31.83	95.9
UCUR-9.1	274.7	41.9	0.153	35	18	5.52311	0.07948	1072.75	28.10	84.1
UCUR-14.1	141.0	64.2	0.455	18	2	7.63582	0.07053	793.35	104.03	94.1

Shrimp UCUR-03

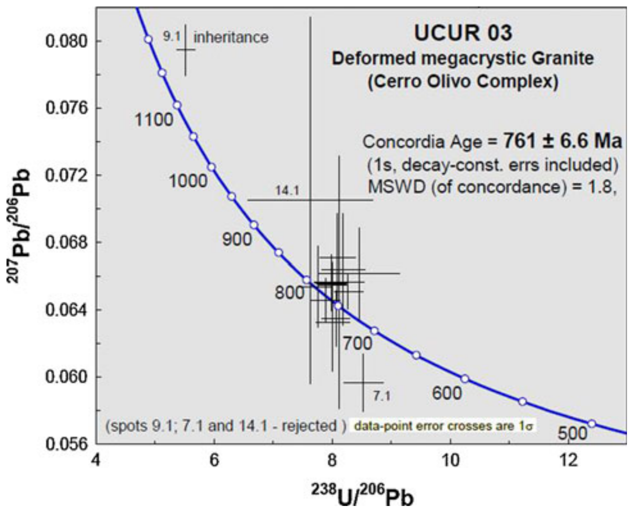

Fig. 5 $^{238}U/^{206}Pb$ versus $^{207}Pb/^{206}Pb$ concordia plot for sample UCUR-03. Analytical errors are depicted at the 1 sigma level

Masquelin et al. (2001) proposed that the basement of the PET should be known as the Cerro Olivo Gneissic Complex, recognizing its Neoproterozoic high-grade metamorphic (granulite facies) and polydeformational condition. The Cerro Olivo Complex contains three major units: (a) the Sierra de Centinela Suite, the youngest one, represented by porphyroclastic metagranites, metagranodiorites and two-mica migmatites; (b) the Cerro Bori orthogneisses with tonalitic to dioritic compositions (Fig. 3e), and locally trondhjemitic granitoids and (c) the metasedimentary Chafalote Unit. The latter is the oldest (Gross et al. 2009) and is mostly represented by high-grade paragneisses (Fig. 3a) composed by banded quartzofeldspathic migmatites, garnet-sillimanite-biotite gneisses and calc-silicate rocks. These occur as enclaves in trondhjemites of the Cerro Bori orthogneisses. Metamorphic conditions of ca. 800°C and 4.3–5.8 kbar have been estimated (Masquelin et al. 2001). Additionally, Masquelin and Morales (2003) and Masquelin (2004) suggested a geological correlation between Cerro Olivo Complex and Namaqualand Complex of Namibia.

The main metasedimentary cover in the PET is represented by the Rocha Formation (Fig. 3b), which occurs in a ca. 120 km long, 20–30 km wide, NE-trending belt (Hasui et al. 1975; Preciozzi et al. 1985; Fragoso Cesar et al. 1987; Preciozzi et al. 1993, Sánchez Bettucci and Mezzano 1993). The Rocha Formation is characterized by siliciclastic metasediments (metapelites to metapsammites). They have mostly been affected by greenschist facies metamorphism (chlorite-sericite mineral assemblages), locally with some metamorphic biotite schists. The Rocha Formation underwent polyphase folding and displays NW-plunging structures and eastward tectonic vergence (Masquelin 1990). In lower metamorphic grade domains, there is common preservation of primary structures such as cross and plane-parallel bedding, cross stratification, mud drapes and arenitic levels with graded bedding, and climbing ripples (Pazos and Sánchez Bettucci 1999). These authors suggest a transitional fluvial environment to tidal plain.

There are isolated remains of post-orogenic sedimentary basins. The best example occurs near San Carlos city, where a series of low-grade metasedimentary rocks were intensely affected by the Sierra Ballena Shear Zone. The San Carlos Formation is composed of polymictic metaconglomerates at the base (Fig. 3c), which grade upward to meta-arkoses with intercalated layers of sericitic-schists derived from pelites (Masquelin 1990). Sánchez Bettucci and Pazos (1996) suggested these rocks were deposited in a braided fluvial setting. This sequence is deformed into a syncline.

The Sierra de Aguirre Formation (Masquelin and Tabó 1988; Fantin 2003) with an age of 572 ± 11 Ma (Hartmann et al. 2002) is the best example of a volcano-sedimentary basin in the PET. It consists of intermediate to acidic pyroclastic rocks dominated by ignimbrites of rhyolitic and dacitic composition and diverse tuffs. Its maximum thickness is ca. 1200 m. The Sierra de Aguirre Formation has been divided into three members by Fantin (2003). The bottom member consists of volcanic rocks and minor sedimentary rocks. Sedimentary rocks predominate in the central member but with some ignimbritic units in which fresh obsidian is preserved. The top member consists of feldspathic sandstones and massive pelites, with only rare volcanic rocks. This formation is in tectonic contact with the Cerro Olivo Unit and the Rocha Formation (Sánchez Bettucci et al. 2010a). According to Fantin (2003), this association suggests a shallow-marine deltaic environment. This formation has been folded with a N°30–40°E axial orientation and an axial-planar schistosity.

Numerous intrusive granites are observed along the full extent of the PET, ranging from batholithic bodies to small stocks. They are isotropic and often leucocratic and are the last important magmatic event that affected the PET. The main calk-alkaline granitic complexes are the Santa Teresa and José Ignácio batholiths. The Rocha and Alférez Granites are the most important syn-kinematic intrusions (Masquelin 1990, Muzio and Artur 1999). The tectonic evolution in this terrane is marked by intense Neoproterozoic migmatization and deformation, development of the Rocha basin and a post-collisional basin (Sánchez Bettucci et al. 2010a), and finally post-tectonic granitic magmatism. The major structures have a NE–SW trend and are recognized in the basement and in the Rocha Formation supracrustal rocks (Fig. 2).

Table 2 Sm–Nd and Rb–Sr analytical data

SPU	Fraction	$^{207}Pb/^{235}U$#	2s Error (%)	$^{206}Pb/^{238}U$#	2s Error (%)	$^{207}Pb/^{206}Pb$	2s Error (%)	$^{206}Pb/^{204}Pb$*	Pb (ppm)	U (ppm)	Weight (mg)	$^{206}Pb/^{238}U$	$^{207}Pb/^{235}U$ Ages (Ma)	$^{207}Pb/^{206}Pb$
URPR-75														
2366	(MAG 1.0A) A	0.885727	0.461	0.105061	0.457	0.0611443	0.0572	9,223	1250.1	2115.1	0.0126	644	644	644
2367	(MAG 1.0A) B	0.891775	0.461	0.105608	0.457	0.061243	0.058	1,0841	1198.6	2476.4	0.0112	647	647	648
2368	(MAG 1.0A) C	0.887216	0.463	0.105209	0.459	0.0611614	0.0593	6,580	1938.2	3404.2	0.0064	645	645	645
AC301														
1534	(MAG 1.0A) 1	0.867653	0.571	0.103242	0.544	0.0609519	0.171	2,458	2175.6	1206.6	0.0120	633	634	638
1535	(MAG 1.0A) 2	0.861798	0.73	0.102856	0.696	0.0607682	0.217	2,749	1489.7	1170.0	0.0475	631	631	631
UCUR 3														
	M1	1.27011	0.91	0.122614	0.908	0.075128	0.0619	1,445	56.8	455.5	0.5990	746	832	1,072
	M1 AA	0.972056	0.91	0.096082	0.906	0.0733749	0.0781	317	23.7	206.3	0.9670	591	690	1,024
	M3	1.08382	0.907	0.110204	0.905	0.071328	0.0581	1,118	52.8	466.7	0.8180	674	746	967
	M2	1.30172	0.949	0.131307	0.949	0.071900	0.0836	408	29.8	201.5	0.5870	795	846	983
	M2 AA	1.22101	0.923	0.122879	0.913	0.072068	0.126	265	18.9	124.4	0.5580	747	810	988
URPR26														
321	M–3	0.866638	0.942	0.088551	0.911	0.0709815	0.234	449	140.8	1421.6	0.1300	547	634	957
322	M−4	0.906336	0.946	0.092694	0.914	0.070915	0.23	601	122.9	1224.2	0.1600	571	655	955
323	M−6	1.05707	0.949	0.106843	0.915	0.0717554	0.232	525	94.8	802.3	0.2400	654	723	979
324	M−3.4	1.0479	0.92	0.103695	0.907	0.0732922	0.144	708	52.6	476.4	0.2900	636	728	1,022
1561	M−4	0.850478	0.662	0.0923783	0.631	0.0667717	0.2	1,364	27.2	298.4	0.0699	570	625	831
1562	M−6	1.06121	0.537	0.107474	0.529	0.0716139	0.093	1,251	33.0	303.3	0.1009	658	734	975
	M2	1.30172	0.949	0.131307	0.949	0.0718998	0.0836	408	29.8	201.5	0.5900	795	846	983
	M2 AA	1.22101	0.923	0.122879	0.913	0.0720677	0.126	265	18.9	124.4	0.5600	747	810	988
	M3	1.08382	0.907	0.110204	0.905	0.0713283	0.0581	1,118	52.8	466.7	0.8200	674	746	967
URPR-73														
1997	M (−2)	0.854334	0.52	0.0960794	0.505	0.0644906	0.122	415	63.5	605.1	0.0223	591	627	758
1998	M (−3) A	0.970523	0.475	0.102922	0.469	0.0683908	0.0743	1,635	107.4	1065.6	0.0258	632	689	880
1999	M (−3) B	0.863197	0.495	0.0997857	0.49	0.0627394	0.0741	2,597	69.3	722.8	0.0223	613	632	700
2000	M (−4)	1.13635	0.505	0.114257	0.498	0.0721315	0.0817	3,515	61.1	525.4	0.0297	697	771	990
2001	M(−4)+NM(−4)	0.868124	0.992	0.102627	0.846	0.0613506	0.491	1,360	54.2	544.1	0.0156	630	635	652
2449	M (−1) A	4.02562	3.68	0.253622	3.68	0.115118	0.3890	200	76.4	250.9	0.0031	1,457	1,639	1,882
2450	M (−1) B	6.47055	0.679	0.368826	0.672	0.127434	0.0945	1,220	59.8	146.6	0.0281	2,021	2,042	2,063
2451	M (−1) C	1.10498	1.48	0.105883	1.46	0.0756878	0.214	649	755.8	1086.8	0.0071	649	756	1,087
2452	M (−1) D	0.880697	0.672	0.0996446	0.664	0.064102	0.103	1,416	76.4	795.6	0.0190	612	641	745
2453	M (−2) A	6.49786	4.97	0.370846	4.96	0.127080	0.4060	172	48.4	109.9	0.0037	2,033	2,046	2,058
AC-301														

Table 2 continued

SPU	Fraction	$^{207}Pb/^{235}U$#	2s Error (%)	$^{206}Pb/^{238}U$#	2s Error (%)	$^{207}Pb/^{206}Pb$	2s Error (%)	$^{206}Pb/^{204}Pb$*	Pb (ppm)	U (ppm)	Weight (mg)	$^{206}Pb/^{238}U$	$^{207}Pb/^{235}U$ Ages (Ma)	$^{207}Pb/^{206}Pb$
1383	A	1.05986	0.772	0.117004	0.711	0.0656971	0.297	688	25.9	212.0	0.1115	713	733	796
1384	B	0.966585	1.07	0.110228	1.03	0.0635984	0.287	652	33.2	287.7	0.0849	674	686	728
1385	C	0.949184	1.32	0.107982	1.15	0.0637526	0.648	498	42.3	364.4	0.0860	661	677	733
1386	E	1.03311	0.722	0.114125	0.691	0.0656544	0.206	763	27.4	235.0	0.0866	696	720	795
1387	F	1.00409	0.882	0.115683	0.842	0.0629507	0.248	455	18.7	151.7	0.0840	705	705	706
1517	D	1.00513	0.9	0.108282	0.886	0.0673234	0.154	991	20.9	193.9	0.0493	663	706	848
1566	M−4,−5	1.12891	0.642	0.115529	0.591	0.0708713	0.239	1,109	66.6	556.6	0.0927	704	767	953
AC-366B														
533	<0.074AAA1	1.04081	6.33	0.106096	6.21	0.0711492	1.2	2,000	19.0	178.6	0.1981	650	724	962
534	<0.074B	0.762889	0.784	0.0900276	0.744	0.0614589	0.237	1,934	79.8	881.3	0.1494	556	576	655
1567	M−2	0.882119	0.541	0.0973212	0.531	0.0657383	0.0984	548	83.3	781.9	0.0724	599	642	798

SPU Laboratory number; *Magnetic fractions* Numbers in parentheses indicated the tilt used on Frantz separator at 1.5 amp. *Current* # Radiogenic Pb corrected for blank and initial Pb; U corrected for blank; * Not corrected for blank or non-radiogenic Pb; Total U and Pb concentrations corrected for analytical blank; Ages: given in Ma using Ludwig Isoplot/Ex program (1998), decay constants recommended by Steiger and Jäeger (1977)

Geochronology

The previous geochronological data, based mainly on Rb–Sr determinations, give ages between 680 and 600 Ma for the gneissic-migmatitic rocks and deformed granitoids, whereas the post-tectonic granitoid ages are concentrated around 550 Ma.

Hartmann et al. (2002) presented a SHRIMP U–Pb zircon age of 762 ± 8 Ma for the Rocha syenogranitic gneisses, of the Cerro Olivo Complex, which constitutes the basement in the PET domain. In the same sample, older zircon U–Pb ages were also obtained mainly in the core of zircon grains, and they were interpreted to be pre-igneous inherited xenocrysts. A similar explanation was recently proposed by Oyhantçabal et al. (2009) for the age of 776 ± 12 Ma obtained for another orthogneiss of the same Complex, which led these authors to correlate these rocks with Damara and Kaoko belt pre-rifting events. These authors interpreted the younger ages (641 ± 17 Ma) obtained from zircon rims as the age of high-grade metamorphism and also suggested the interval between 650 and 600 Ma for granitic magmatism. In the same way, theses authors propose a correlation between the PET and the Coastal terrane of the Kaoko belt.

In this work, six samples from the basement of the PET have been analyzed by U–Pb IDTIMS for zircons and monazites (UCUR-03; URPR-26; AC-301; URPR-75; URPR-73; and AC-366B). For sample UCUR-03, SHRIMP U–Pb data are also available.

The samples UCUR-03 and URPR-26 are quartzo-feldspathic biotite-bearing migmatites with deformed K-feldspar megacrysts. Sample AC-301 is an example of a highly evolved peraluminous granodioritic to monzogranitic leucosome. Samples URPR-75 and URPR-73 are sillimanite-garnet bearing paragneisses from which zircons and monazites have been extracted from the mafic layers. AC-366B is a deformed leucogranite.

SHRIMP U–Pb zircon analysis

SHRIMP U–Pb zircon analyses were performed at the Research School for Earth Sciences at the Australian National University, Canberra. Zircons were handpicked, mounted in epoxy resin and polished. Transmitted and reflected light microscopy as well as SEM cathodoluminescence imagery was used to determine the internal structures of the zircons prior to analysis. Data were collected and reduced as described by Compston et al. (1984) and Williams (1998). Ages were calculated from the $^{206}Pb/^{238}U$ ratios after corrections for the appropriate Cumming and Richards (1975) composition of common Pb for rock formation ages and are presented at the 95% confidence level. All the geochronological statistical

Fig. 6 Photographs of selected UCUR-03 zircons analyzed by IDTIMS

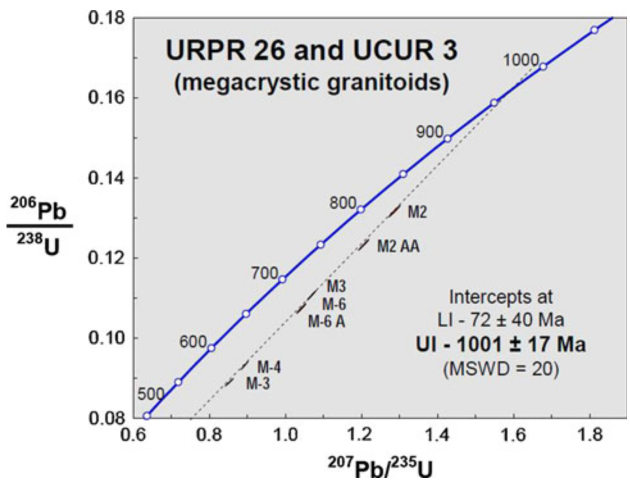

Fig. 7 $^{238}U/^{206}Pb$ versus $^{207}Pb/^{206}Pb$ concordia plot for zircon data from UCUR-03 and URPR-26 megacrystic granites (IDTIMS data). Analytical errors are depicted at the 2 sigma level

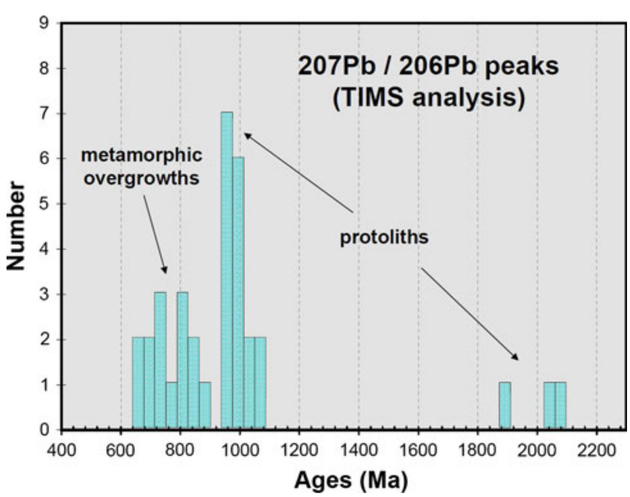

Fig. 8 Histogram summarizing Mesoproterozoic protholith ages

assessments were made using the Isoplot/Ex program of Ludwig (2001).

In Fig. 4, the cathodoluminescence images of representative dated UCUR-03 zircons are presented. Most ages were obtained in the outmost parts of the grains, aiming at the characterization of the last important thermal event that led to the rock formation. Additionally, an age of ca. 1,070 Ma was obtained from inherited nuclei. Most of zircons are homogeneous, rounded to ovoid surrounded by metamorphic overgrowths rims, some present inherited igneous cores showing relicts of oscillatory zoning (Fig. 4). Fifteen analyses of UCUR-03 zircons are presented in Table 1, and the data are shown on a concordia plot (Fig. 5). Two core analyses (9.1 and 14.1) indicate the oldest ages, with site 9.1 showing a $^{206}Pb/^{238}U$ age of 1,073 ± 28 Ma (1 sigma). The $^{206}Pb/^{238}U$ 761 ± 7 Ma age on the main population ($MSWD = 1.8$) is interpreted as the time of crustal melting episode related to the formation of the UCUR-03 protolith. The ca. 1,070 Ma xenocrysts indicate igneous Mesoproterozoic materials in the source region.

The above interpretation is in agreement with the SHRIMP data presented by Hartmann et al. (2002) and Oyhantçabal et al. (2009) which however show dispersion of analytical points in the concordia plots. The latter authors characterized a concordant age of 641 ± 17 Ma for the overgrowths around the 776 Ma older nuclei. These overgrowths are well characterized in the CL images (Fig. 4), giving evidence of a second Neoproterozoic thermal event. The peak P–T conditions linked to the ca. 640 Ma metamorphic event is ca. 830–950°C and 7–10 kbar (Masquelin 2000; Gross et al. 2009).

TIMS U–Pb zircon analysis

Following zircon separation by standard Wilfley table, heavy liquid and isodynamic techniques, grains for analysis were selected with a stereomicroscope. After chemical abrasion, the dissolution of the zircon crystals was carried out with HF and HNO_3 in Teflon beakers in which a mixed $^{205}Pb/^{235}U$ spike was added. A set of 15 beakers arranged in a metal jacket is left for three days in a stove at 200°C. U and Pb are concentrated and purified by passing the solution in an anionic exchange resing column. The concentration and purification of U and Pb were carried out by passing the solution in ion-exchange columns, according to

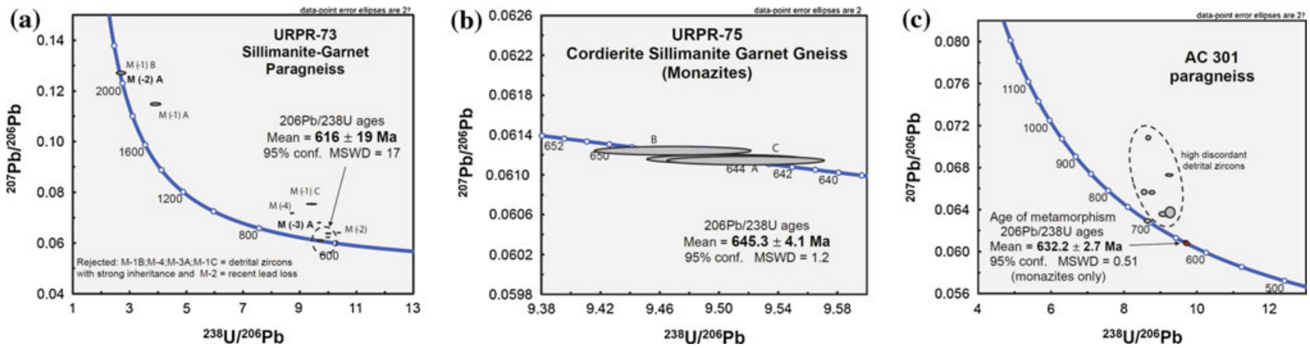

Fig. 9 $^{238}U/^{206}Pb$ versus $^{207}Pb/^{206}Pb$ concordia plot of **a** URPR-73 **b** URPR-75 and **c** AC-301 samples (IDTIMS data). Analytical errors are depicted at the 2 sigma level

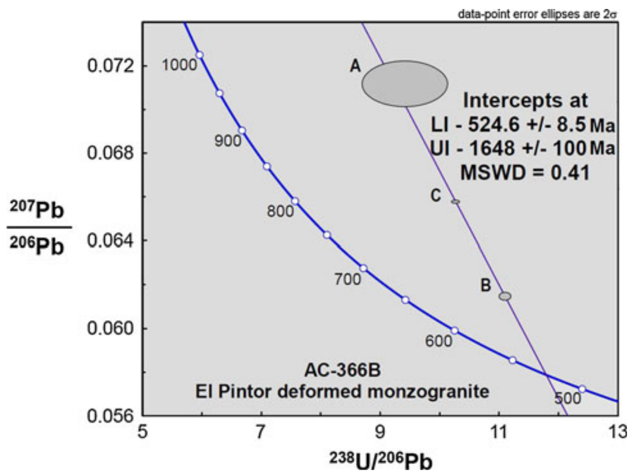

Fig. 10 $^{238}U/^{206}Pb$ versus $^{207}Pb/^{206}Pb$ concordia plot for the El Pintor Granite (IDTIMS data). Analytical errors are depicted at the 2 sigma level

the method of Krogh (1973). The isotopic analyses were obtained with a multi-collector MAT 262 mass-spectrometer. The ages were calculated using the PbData software of Ludwig (2001) after correction of the spectrometric ratios for isotopic fractionation, laboratory blank and initial lead. In all samples, at least two types of zircons were recognized. The analytical procedure is described in detail by Passarelli et al. (2009). Summary analytical data are presented in Table 2.

In UCUR-03 and URPR-26, the predominant zircon type selected for analysis were pink to clear translucent prisms with bipyramidal terminations (mostly with a 2–3:1 aspect ratio), devoid of inclusions and with as few fractures as possible (Fig. 6). In general, they display rounded edges. Several fractions were abraded with intervals varying from 4 to 8 h. Figure 7 presents the concordia plot (Whetherill 1956; Wasserburg 1963) of URPR-26 and URUC-03 analyses. Both samples yielded similar arrays of discordant data and thus were pooled to calculate ages. An upper intercept of 1,001 ± 17 Ma (*MSWD* = 20) was obtained, definitely younger than the ≥1,073 ± 28 Ma age for pre-igneous xenocrysts obtained by SHRIMP U–Pb analysis on UCUR-03 zircons. Therefore, the IDTIMS data represent complex mixtures between ≥1,073 Ma xenocrysts, and zircon grown during Neoproterozoic igneous and metamorphic events. Nonetheless, the ca. 1,000 Ma IDTIMS age is additional strong evidence for Mesoproterozoic rocks in the PET. It is considered here that the main rock formation episode in the PET basement occurred at ca. 760 Ma, as indicated by the SHRIMP U–Pb ages on UCUR-03 igneous zircon. Therefore, due to the intensity of the deformation and thermal Neoproterozoic overprint, pre-Brasiliano rocks surrounded by the Brasiliano gneisses and granitoids including the Mesoproterozoic ones are highly obliterated. The concentration of the analytical points far from the upper intercept (Fig. 7) reflects an isotopic disequilibrium of the Mesoproterozoic protholiths during the Brasiliano/Pan-African orogenesis. Due to the air ablation treatment that caused the elimination of Brasiliano zircon overgrowths, the Mesoproterozoic older ages were better characterized when TIMS techniques were used (Fig. 8). On the other hand, the overgrowths were an easy target during the SHRIMP studies.

Sample URPR-73 is a cordierite–sillimanite–garnet paragneiss. Zircon analyses cluster close to a lower intercept (Fig. 9a) and is considered to be a mixture of (high-U) zircon grown during regional metamorphism and detrital cores. Extrapolation to an upper intercept indicates an average Paleoproterozoic age (2,070 Ma) for the detrital component. Peak Neoproterozoic metamorphism is dated by monazite at 645 ± 4 Ma (*MSWD* = 1.2; sample URPR-75, Fig. 9b) and at 632 ± 3 Ma (*MSWD* = 0.51; sample AC-301, Fig. 9c). These monazite ages are in good agreement with the SHRIMP U–Pb age of ca. 641 Ma for zircon metamorphic overgrowths (Oyhantçabal et al. 2009). Leucosome sample AC-301 (Fig. 3d) presents, among several high discordant analysis a zircon concordant fraction with U–Pb age of a 704 ± 17 Ma, suggesting that the analyzed grains is a mixture of several inherited zircon

Table 3 U-Pb IDTIMS analytical data

Sample	Sm (ppm)	Nd (ppm)	$^{147}Sm/^{144}Nd$	$^{143}Nd/^{144}Nd$	$\varepsilon_{(0)}$	T_{DM} (Ma)	$\varepsilon_{(TDM)}$	T_1 (Ma)	$\varepsilon_{(T1)}$
URPR-26	6.94	29.10	0.1442	0.511971	−13.01	1.96	2.80	1,000	−6.32
URPR-30	7.58	32.00	0.1432	0.511949	−13.44	1.98	2.77	1,000	−6.62
URPR-33	6.73	32.00	0.1272	0.511915	−14.10	1987.1	3.52	600	−8.78
URPR-35	6.18	34.10	0.1096	0.511991	−12.62	1538.2	4.47	600	−5.95
URPR-36	9.50	48.60	0.1182	0.511905	−14.30	1814.7	3.87	600	−8.29
URPR-73	10.76	53.90	0.1207	0.511803	−16.29	2033.0	3.43	650	−9.99
URPR-75	14.46	79.26	0.1104	0.511541	−21.40	2220.9	3.06	650	−14.24
URPR-76	12.07	55.98	0.1304	0.511904	−14.32	1860.0	3.32	650	−8.82
URPR-72	7.85	38.79	0.1224	0.511921	−13.98	1870.9	3.76	650	−7.82

Sample	Rb (ppm)	Sr (ppm)	$^{87}Rb/^{86}Sr$	$^{87}Sr/^{86}Sr$	ε(0)	T_1 (Ma)	$\varepsilon(T_1)$	Ri
URPR-26	215.00	74.90	8.4187	0.84317	1968.4	1,000	276.4	0.72278
URPR-30	4.70	492.00	0.0277	0.72125	237.7	1,000	249.1	0.72085
URPR-33	88.00	85.90	2.9751	0.74259	540.6	600	189.4	0.71713
URPR-35	94.00	88.80	3.0732	0.73948	496.5	600	133.2	0.71318
URPR-36	207.00	80.80	7.4797	0.79683	1310.5	600	412.4	0.73283
URPR-73	137.16	91.62	4.3605	0.77331	976.7	650	413.9	0.73287
URPR-75	93.25	262.16	1.0325	0.73742	467.2	650	342.4	0.72784
URPR-76	44.82	197.35	0.6584	0.72490	289.5	650	213.9	0.71879
URPR-72	261.09	80.24	9.5264	0.82496	1709.9	650	467.2	0.73662

(URPR-26: −34°15′00.108″, −54°25′57.062″; URPR-30: 34°22′04.861″, −54°30′24.101″; URPR-33: −34°37′31.636″, −54°10′32.181″; URPR-35: −34°33′10.546″, −54°08′39.608″; URPR-73: −34°54′42.52″, −54°49′35.322″; URPR-75: −34°30′41.415″, −54°26′20.934″; URPR-76: −34°29′07.463″, −54°31′35.964″; UCUR-03: −34°24′38.587″, −54°17′57.837″; AC301: −34°20′55.666″, −54°23′53.924″; AC366B: −34°20’0.89″, −54°42’44.72″)

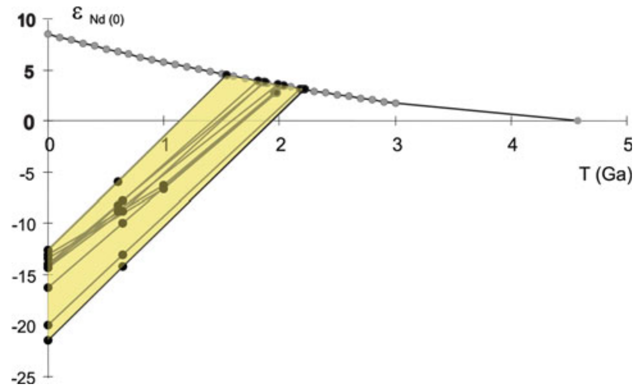

Fig. 11 εNd versus T diagram (DePaolo 1988)

components overprinted by ca. 640 Ma metamorphic episode as indicated by the monazite ages (Fig. 9c).

Sample AC-366B is of the post-tectonic El Pintor monzogranite. This intrudes previously deformed gneisses but has been deformed in the Alférez-Cordillera Shear Zone (Fig. 3f). The 524.5 ± 8.6 Ma ($MSWD = 0.41$) lower intercept value is interpreted as the emplacement age of the El Pintor granitoid, whereas the poorly defined Mesoproterozoic upper intercept of 1,648 ± 100 Ma could indicate the age for inherited zircon xenocrysts from the source materials (Fig. 10).

Nd and Sr isotopic data

The Nd and Sr isotopic data were obtained on nine rocks to constrain further the origin of the material involved in the formation of the PET. These included two metapsammitc rocks of the Rocha Formation and some samples also used for U–Pb mineral analysis. The isotopic ratios of $^{87}Sr/^{86}Sr$ and $^{143}Nd/^{144}Nd$ were measured by thermal ionization mass spectrometry at Centro de Pesquisas Geocronologicas/USP. Detailed description of analytical procedure and equipments is presented at http://www2.igc.usp.br/cpgeo/laboratorios.phc. The analytical data are presented in Table 3.

Samples show negative εNd values of −1.3 and –14.3 and Palaeoproterozoic (2,200–1,800 Ma) T_{DM} model ages. Results are summarized in a εNd versus time diagram (Fig. 11). Similar values have been found for Namaquan metamorphic rocks in southwestern Africa (Eglington 2006). The εNd versus εSr diagram (Fig. 12) with the data recalculated to 635 Ma, (the time of peak metamorphism when Rb–Sr fractionation might have occurred) shows clearly negative εNd and positive εSr values. This again suggests no addition of juvenile crustal material in the Neoproterozoic. Additionally, the involvement of the upper crust in the generation of most of the analyzed rocks can be characterized by the slight to medium negative εNd values and the large distribution of εSr values, between 100 and 500, which is explained by the presence of lithophile elements, suggesting enriched continental crust.

Conclusions

Based on the available geological and radiometric data, the following evolution for the Punta del Este Terrane (PET) is proposed (Table 4):

Mesoproterozoic (1,100–900 Ma) U–Pb ages were obtained on inherited cores of zircon grains from the PET basement rocks. These ages support the interpretation that

Fig. 12 Diagram εNd versus εSr (recalculated for 600 Ma)

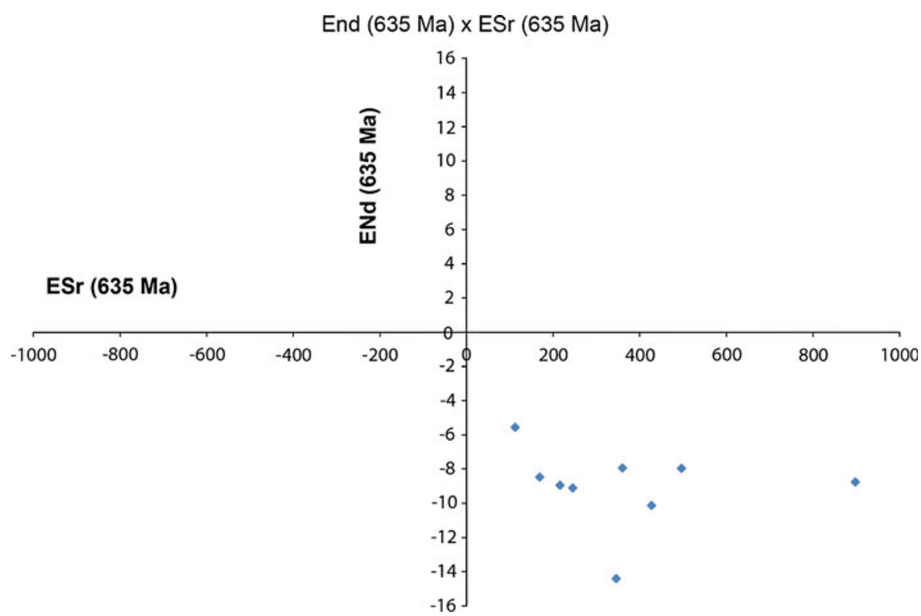

Table 4 Major chronostratigraphic units of the PET with the available radiometric control

Unit	Main type
Post-tectonic granites	El pintor (ca. 525 Ma)[a]
	Santa teresa batholith (537 ± 7/556 ± 7* Ma)[b]
Volcano-sedimentary basins	San carlos and sierra de aguirre formations (571 ± 8 ma)[d]
Syn-to late-tectonic granites	José ignacio (590 ± 25 Ma/611 ± 25 Ma*)[b]
	Garzón (601 ± 20 Ma)[c]
	Valdivia (636 ± 6 Ma)[c] florencia (591 ± 95 Ma)[c]
Metasedimentary sequence	Rocha formation (younger detrital zircon ages 629 ± 17, 668 ± 20, 670 ± 18, and 714 ± 20)[e]
High-grade metamorphism	Migmatites and gneisses (641 ± 17 Ma)[a, f]
	Sierra de los Caracoles (681 ± 48 Ma)[c]
	Alférez (670 ± 49 Ma)[c]
	Rocha syenogranite (gneisses) (678 ± 14[c]/747 ± 6[d] Ma)
Basement ortho and paragneiss (ca 1.0 Ga mesoproterozoic protoliths)	Cerro olivo complex: sierra centinela, cerro bori and chafalote units (ca. UI 1000/LI 760 Ma)[a]

[a] This work

[b] Umpierre and Halpern (1971)

[c] Preciozzi et al. (1993)

[d] Hartmann et al. (2002)

[e] Basei et al. (2005)

[f] Oyhantçabal et al. (2009)

*Ages** Recalculated ages using decay constants reported by Steiger and Jäeger (1977)

this unit represents a remnant of Namaqua belt of Namibia and South Africa preserved in Uruguay.

The oldest U–Pb zircon igneous ages of 750 ± 50 Ma obtained from deformed granitoids of the PET basement indicate crustal melting of Mesoproterozoic protoliths, as suggested by the ca 1,000 Ma inherited zircon cores. Old Sm–Nd model ages and strong negative ε_{Nd} values also indicate a strong pre-Neoproterozoic contribution to these rocks. This event is probably related with the extension associated with the opening of the Adasmastor Ocean (sensu Frimmel et al. 2001).

A regional high-grade metamorphic episode at ca. 635 ± 10 Ma (concordant SHRIMP U–Pb zircon and ID-TIMS U–Pb monazite ages) migmatized and gneissified the PET basement. An extensional phase with the development of volcano-sedimentary post-collisional basins (Sierra de Aguirre and San Carlos formations) developed at ca. 570 Ma. The deformation of these basins and the final emplacement alongside the Dom Feliciano belt occurred before intrusion of the Santa Teresa Granite (537 Ma, Umpierre and Halpern 1971). This interpretation is in accordance with paleomagnetic data (Rapalini and Sánchez Bettucci 2008) from the Lavalleja and Arroyo del Soldado Groups (sensu Sánchez Bettucci et al. 2010a). Rapalini and Sánchez Bettucci (2008) found a remagnetization event at ca. 525 Ma which could represent an important tectono-thermal event affecting the eastern Uruguay.

In conclusion, the Neoproterozoic evolution of the PET is associated with crustal reworking of Mesoproterozoic rocks, involving major ca. 750 Ma extension followed by a ca. 635 ± 10 Ma compressional high-grade metamorphic event linked to collisional orogeny. Post-collisional extension occurred between 580 and 570 Ma, as represented by the emplacement of post-tectonic granites and development of volcano-sedimentary basins. The final juxtaposition between the PET and the western South American terranes occurred at ≤535 Ma.

Based on the available radiometric data, correlation between the PET (basement and cover) and parts of the African Namaqua and Gariep belts is emphasized. Most compelling for this correlation is the 1,000–750 Ma U–Pb zircon ages observed in the basement rocks of both sides of south Atlantic (see also Hartmann et al. 2002; Oyhantçabal et al. 2009, 2010a). Other authors (Oyhantçabal et al. 2009; Goscombe and Gray 2009) suggest the correlation with the Coastal terrane of the Kaoko belt based on the coeval metamorphism and magmatism, which is hard to find at the same crustal level. Throughout the PET, the Neoproterozoic reworking was much more intense than in Namaqua belt, where migmatites and granitoids were formed by crustal melting of previous Mesopoterozoic rocks.

Acknowledgments The authors thank Fundação de Amparo à Pesquisa do Estado de São Paulo (FAPESP) for the financing support (process N° 05/58688-1) which covered part of the costs with field-work and isotopic analyses. Several grants Consejo Sectorial de Investigación Científica (CSIC) and Facultad de Ciencias (Uruguay) permitted to carry out these studies. EP thanks CAPES for granting a PhD. Scholarship. We express our sincere thanks to P. Oyhantçabal for his comments and suggestions. We are also grateful to Dr. Klaus Wemmer and two anonymous referees for their critical review and comments to the manuscript.

References

Basei MAS, Siga O Jr, Masquelin H, Harara OM, Reis Neto JM, Preciozzi F (2000) The Dom Feliciano Belt (Brazil-Uruguay) and its foreland domain, the Rio de la Plata craton: framework, tectonic evolution and correlation with similar provinces of Southwestern Africa. In: Cordani UG, Milani EJ, Thomaz Filho A, Campos DA (eds) Tectonic Evolution of South America. 31 Int Geol Congress. Rio de Janeiro, Brazil, pp 311–334

Basei MAS, Frimmel HE, Nutman AP, Preciozzi F, Jacob J (2005) A connection between the Neoproterozoic Dom Feliciano (Brazil/Uruguay) and Gariep (Namibia/South Africa) orogenic belts–evidence from a reconnaissance study. Precambrian Res 139:195–221

Basei MAS, Frimmel HE, Nutman AP, Preciozzi F (2008) West Gondwana amalgamation based on detrital zircon ages from Neoproterozoic Ribeira and Dom Feliciano belts of South America and comparison with coeval sequences from SW Africa. In: west gondwana pre-cenozoic correlations across the south Atlantic region. RJ Pankhurst, RA Trown, BB de Brito Neves, MJ de Wit (eds) Geol Soc S Pub, vol 294: pp 239–256

Becker T, Schreiber U, Kampunzu AB, Armstrong R (2006) Mesoproterozoic rocks of Namibia and their plate tectonic setting. J Afr Earth Sci 46:112–140

Bitencourt MF, Nardi LVS (2000) Tectonic setting and sources of magmatism related to the Southern Brazilian shear belt. Rev Bras Geoc 30:184–187

Bossi J, Campal N (1992) Magmatismo y tectónica transcurrente durante el paleozoico inferior en Uruguay. In: Gutierrez-Marco JG, Saavedra J, Rabano I (eds) Paleozoico inferior de iberoamérica, Universidad de ExtremaduraRev Bras Geoc, pp 343–356

Bossi J, Cingolani C (2009) Extension and General evolution of the Rio de La Plata Craton. In: Gaucher C, Sial AN, Halverson GP, Frimmel HE (eds) Neoproterozoic Tectonics, Global Change and Evolution: A Focus on Southwestern Gondwana. Chapter 4.1. Elsevier, Amsterdam

Bossi J, Navarro R (1988) Geología del Uruguay. Depto. Publ. Universidad República, Montevideo, t. I, p 453

Bossi J, Hartmann LA, Piñeyro D, Leite JAD, McNaughton NJ (1999) Geological and geochronological constraints on the paleoproterozoic evolution of the Isla Mala granitic suite, Uruguay. II South American symposium on isotope geology, Actas, Cordoba, Argentine, pp 295–299

Chemale F Jr (2000) Evolução geológica do Escudo Sul-riograndense. In: Holz M, De Ros LF (eds) Geologia do Rio Grande do Sul. Porto Alegre: CIGO/UFRGS S Pub, 444p l: pp 13–52

Cingolani C, Spoturno J, Bonhomme M (1990) Resultados mineralógicos y geocronológicos sobre las unidades Piedras de Afilar, Lavalleja y Barriga Negra. Rep.Oriental del Uruguay. In: Primer Congreso Uruguayo de Geología 1:11–24

Clifford TN, Stumpfl EF, Burger AJ, McCarthy TS, Rex DC (1981) Mineral-chemical and isotopic studies of Namaqua granulites, South Africa: a Grenville analogue. Contrib Mineral Petrol 77:225–250

Compston W, Williams IS, Meyer C (1984) U-Pb geochronology of zircons from lunar breccia 73217 using a sensitive high mass-resolution ion microprobe. J Geoph Res 89:525–534

Cordani UG, D'Agrella-Filho MS, Brito Neves BB, Trindade RIF (2003) Tearing up Rodinia: the Neoproterozoic palaeogeography of South American cratonic fragments. Terra Nova 15:350–359

Cumming GL, Richards JR (1975) Ore lead ratios in a continuously changing Earth. Earth Planet. Sci Lett 28:155–171

DePaolo DJ (1988) Neodymium isotope geochemistry: an introduction. Springer, Berlin Heidelberg, Germany, p 187

Eglington BM (2006) Evolution of the namaqua-natal belt, southern Africa: a geochronological and isotope geochemical review. J Afr Earth Sci 46:93–111

Fantin M (2003) Geología de la sierra de aguirre, departamento de rocha, Uruguay. Unpublished work submitted for the degree of geologist. University of Buenos Aires, Argentina, p 92

Florisbal LM, Bitencourt MF, Nardi LVS, Conceição RV (2009) Early post-collisional granitic and coeval mafic magmatism of medium- to high-K tholeiitic affinity within the Neoproterozoic Southern Brazilian shear belt. Precambrian Res 175:135–148

Fragoso Cesar ARS (1991) Tectonica de Placas no Ciclo Brasiliano: as orogenias dos cinturões Dom Feliciano e Ribeira no Rio Grande do Sul. Unpublished Ph.D thesis. University of São Paulo, São Paulo, p 367

Fragoso Cesar ARS, Machado R, Gomés Rifas C (1987) Observações sobre o cinturão dom feliciano no escudo uruguaio e correlações com o escudo do rio grande do Sul. In: III Symposium Sul-Brasileiro de Geologia, Curitiba vol 2: pp 791–809

Frimmel HE (1995) Metamorphic evolution of the Gariep belt. S Afr Tydskr Geol 98:176–190

Frimmel HE (2000) The Pan-African gariep Belt in southwestern Namibia and western South Africa. Commun Geol Survey Namibia 12:197–209

Frimmel HE, Hartnady CJH (1992) Blue amphiboles and their significance for the metamorphic history of the Pan-African Gariep belt, Namibia. J Metamorph Geol 10:651–669

Frimmel HE, Zartman RE, Späth A (2001) Dating neoproterozoic continental break-up in the Richtersveld igneous complex, South Africa. J Geol 109:493–508

Fuck R, Brito Neves BB, Schobbehaus C (2008) Rodinia descendants in South America. Prec Res 160:108–126

Gaucher C, Sial AN, Halverson GP, Frimmel HE (2009a) The Neoproterozoic and Cambrian: a time of upheavals, extremes and innovations. In: Gaucher C, Sial AN, Halverson GP, Frimmel HE (eds) Neoproterozoic-cambrian tectonics, global change and evolution: a focus on southwestern Gondwana. Elsevier, Amsterdam, pp 3–11

Gaucher C, Frimmel HE, Germs GJB (2009b) Tectonic events and palaeogeographic evolution of southwestern gondwana in the neoproterozoic and cambrian. In: Gaucher C, Sial AN, Halverson GP, Frimmel HE (eds) Neoproterozoic tectonics, global change and evolution: a focus on Southwestern gondwana. Elsevier, Amsterdam, pp 295–316

Goscombe BD, Gray DR (2009) Metamorphic response in orogens of different obliquity, scale and geometry. Gondwana Res 15:151–167

Gross AOMS, Droop GTR, Porcher CC, Fernandes LAD (2009) Petrology and thermobarometry of mafic granulites and migmatites from the Chafalote metamorphic suite: new insights into the Neoproterozoic P–T evolution of the Uruguayan–sul-rio-grandense shield. Precambrian Res 170:157–174

Hartmann LA, Santos JO, Bossi J, Campal N, Schiplov A, McNaughton N (2002) Zircon and titanite U-Pb SHRIMP geochronology of Neoproterozoic felsic magmatism on the eastern border of the Rio de La Plata Craton, Uruguay. J S Am Earth Sci 15:229–236

Hasui Y, Carneiro C, Coimbra AM (1975) The Ribera Folded Belt Rev. Bras Geoc 5:257–266

Koester E, Soliani E Jr, Leite JAD, Hartmann LA, Fernandes LAD, McNaughton NJ, Santos JOS, de Oliveira LD (2001) SHRIMP

U-Pb age for the emplacement of the santana granite and reactivation of the porto alegre suture, southern Brazil. J S Am Earth Sci 14:91–99

Krogh TE (1973) A low contamination method for hydrothermal decomposition of zircon and extraction of U and Pb for isotopic age determinations. Geochim Cosmochim Acta 37:485–494

Kröner A (1974) Late Precambrian formations in the western Richtersveld, Northern Cape province. Precambrian research unit, University of Cape Town. ISBN: 0799201162

Li ZX, Bogdanova SV, Collins AS, Davidson A, de Waele B, Ernst RE, Titzsimons ICW, Fuck RA, Gladhchub DP, Jacobs J, Karlstrom KE, Lu S, Natapov LM, Pease V, Pisarevsky SA, Thrane K, Vernikovsky V (2008) Assembly, configuration and break-up history of Rodinia: a synthesis. Prec. Res. 160:179–210

Ludwig KR (2001) Using Isoplot/Ex. A geochronological toolkit for Microsoft Excel. Berkeley Geochronology Center, Special Publications No. 1. Berkeley, USA

Mallmann G, Chemale F, Avila JN, Kawashita K, Armstrong RA (2007) Isotope geochemistry and geochronology of the Nico Perez Terrane, Rio de la Plata Craton, Uruguay. Gondwana Res 12:489–508

Masquelin E (1990) Analisis estructural de las zonas de cizalla en las migmatitas de Punta del Este, Uruguay. Actas Geol Leopold 12:139–158

Masquelin HC (2000) A Evolução Estrutural e Metamórfica do Terreno Punta del Este Sudeste Uruguaio. Unpubl. Tese de Doutorado, Universidade Federal do Rio Grande do Sul, p 350

Masquelin H (2004) Estratigrafía de rocas ‘no estratificadas’ en Uruguay: Hacia un modelo dinámico para su explicación geológica: Revista de la Sociedad Uruguaya de Geología. III Época, Special Number, CD version, Montevideo

Masquelin H, Morales E (2003) El Terreno punta del este: estructura, trayectoria P-T-t, geocronología y su relación con terrenos adyacentes In: Fernandes LAD, Vujovich GI (eds) Simpósio Internacional ‘Acresção Do Microcontinente Cuyania A Proto-Margem Do Gondwana’, Porto Alegre (RS), p 10

Masquelin H, Tabó F (1988) Memoria explicativa de la carta geológica del Uruguay, Hoja chafalote, Escala 1:100.000: DI.NA.MI.GE/Fac. de Agron. Fac. de H. y Cs, p 1–20

Masquelin H, Silva M, Porcher CC, Fernandes LAD (2001) Geología y geotermobarometría de la Suite Metamórfica Chafalote, Basamento Prebrasiliano, Sureste del Uruguay: XI Congreso Latinoamericano de Geologia (CD), Montevideo

McCourt S, Hanson R, Key R (2006) Mesoproterozoic orogenic belts in southern and central Africa. J Afr Earth Sci 46:v-xi

Muzio R, Artur CA (1999) Petrological features of the Santa Teresa Granitic Complex Southeastern Uruguay. J S Am Earth Sci 12:501–510

Oyhantcabal P, Siegesmund S, Wemmer K, Presnyakov S, Layer P (2009) Geochronological constraints on the evolution of the southern Dom Feliciano Belt (Uruguay). J Geol Soc London 166:1075–1084

Oyhantçabal P, Siegesmund S, Wemmer K, Sánchez Bettucci L (2005) The evolution of sierra ballena shear zone (dom feliciano belt) and its correlation with the purros shear zone (kaoko belt): gondwana 12: geological and biological heritage of Gondwana. Abstracts, Argentina, p 97

Oyhantçabal P, Siegesmund S, Wemmer K (2010a) The Rio de La Plata craton: a review of units, boundaries, ages and isotopic signature. Int J Earth Sci. (Geol. Rundsch) doi:10.1007/s00531-010-0580-8

Oyhantçabal P, Siegesmund S, Wemmer K, Layer P (2010b) The sierra ballena shear zone in the southernmost dom feliciano belt (Uruguay): evolution, kinematics, and deformation conditions. Int J Earth Sci (Geol Rundsch) vol 99: pp 1227–1246 doi: 10.1007/s00531-009-0453-1

Oyhantçabal P, Siegesmund S, Wemmer K, Passchier, CW (2010c). The transpression connection between dom feliciano and kaoko belts at 580–550 Ma. Int J Earth Sci (Geol Rundsch) doi: 10.1007/s00531-010-0577-3

Passarelli CR, Basei MAS, Siga O Jr, Sato WM, Sproesser K, Lois V (2009) Dating minerals by ID-TIMS geochronology at times of in situ analysis: selected case studies from the CPGeo-IGc-USP laboratory. An Acad Bras Ciênc 81:73–97. ISSN 0001-3765

Pazos P, Sánchez Bettucci L (1999) Rasgos Maréales en la sucesión neoproterozoica de la Pedrera, Grupo Rocha, Uruguay. XIV Congreso Geol Arg 1:71

Porada H (1979) The damara-ribeira orogen of the Pan-African-Brasiliano cycle in Namibia (Southwest Africa) and Brazil as interpreted in terms of continental collision. Tectonophysics 57:237–265

Preciozzi F, Spoturno J, Heinzen W (1979) Carta Geo-estructural del Uruguay a escala 1/2.000.000. Instituto Geológico Ing. Eduardo Terra Arocena, Montevideo, p 62

Preciozzi F, Spoturno J, Heinzen W, Rossi P (1985) Carta Geológica del Uruguay a escala 1:500.000: Dirección Nacional de Minería y Geología, p 92

Preciozzi F, Masquelin E, Sánchez Bettucci L (1993).Geología de la porción sur del cinturón cuchilla dionisio. In: Preciozzi F, Masquelin E, Sánchez L (eds) guia de excursión del primer simposio internacional del Neoproterozoico-Cambrico de la cuenca del plata, Dirección Nacional de Minería y Geología pp 1–37

Preciozzi F, Masquelin H, Basei MAS (1999) The namaqua/grenville terrane of eastern Uruguay: 2nd South American symposium on isotope geology, Argentina, pp 338–340

Ramos VA (1988) Late proterozoic-early paleozoic of South America: a collisional history. Episodes 11(3):168–173

Rapalini AE, Sánchez Bettucci L (2008) Widespread remagnetization of late proterozoic sedimentary units of Uruguay and the apparent polar wander path for the Rio de La Plata Craton. Geophys J Int 174:55–74

Rapela CW, Pankhurst RJ, Casquet C, Fanning CM, Baldo EG, González-Casado JM, Galindo C, Dahlquist J (2007) The Río de la Plata craton and the assembly of SW Gondwana. Earth-Science Rev 83:49–82

Robb LJ, Armstrong RA, Waters DJ (1998) Nature and duration of mid-crustal granulite facies metamorphism and crustal growth: evidence from single zircon U-Pb geochronology in Namaqualand, South Africa. Economic geology research unit, University of Witwatersrand, South Africa. Information Circular No. 323, p 38

Sánchez Bettucci L, Mezzano A (1993) Análisis sedimentológico y faciológico de la Formación Rocha (ex Grupo Rocha). Rev Bras Geoc 23:323–329

Sánchez Bettucci L, Pazos P (1996) Análisis Paleoambiental y Marco tectónico en la Cuenca Playa Verde, Piriápolis, Uruguay: XII Congreso Geológico Argentino and III Congreso de Exploración de Hidrocarburos. Buenos Aires 1:405–412

Sánchez Bettucci L, Cosarinsky M, Ramos VA (2001) Tectonic setting of the late proterozoic lavalleja group (Dom Feliciano Belt), Uruguay. Gondwana Res 4:395–407

Sánchez Bettucci L, Oyhantçabal P, Page S, Ramos VA (2003) Petrography and Geochemistry of the Carapé Complex, Southeastern Uruguay. Gondwana Res 6:89–105

Sánchez Bettucci L, Peel E, Masquelin H (2010a) Neoproterozoic tectonic synthesis of Uruguay. Int Geol Rev 52(1):51–78

Sánchez Bettucci L, Peel E, Oyhantçabal P (2010b) Precambrian geotectonic units of the Río de La Plata craton. Int Geol Rev 52(1):32–50

Schmitz MD, Bowring SA (2004) Lower crustal granulite formation during Mesoproterozoic Namaqua-Natal collisional orogenesis, southern Africa. S Afr J Geol 107:261–284

Steiger RH, Jäeger E (1977) Subcommission on geochronology: Convention on the use of decay constants in geo- and cosmochronology. Earth Planet Sci Lett 36:359–362

Tack L, Fernandez-Alonso M, Tahon M, Wingate MTD, Barritt S (2002) The "northeastern Kibaran belt" (NKB) and its mineralisations reconsidered: new constraints from a revised lithostratigraphy, a GIS-compilation of existing geological maps and a review of recently published as well as unpublished igneous emplacement ages in Burundi. In: Namibia GSO (ed) 11th IAGOD quadrennial symposium and geocongress. Geological Survey of Namibia, Namibia, p 6

Thomas RJ, Cornell DH, Moore JM, Jacobs J (1994) Crustal evolution of the namaqua-natal metamorphic province, Southern Africa. S Afr J Geol 97:8–14

Tohver E, D'Agrella-Filho MS, Trindade RI (2006) Paleomagnetic record of Africa and South America for the 1200–500 Ma interval, and evaluation of Rodinia and Gondwana assemblies. Precambr Res 147:193–222

Umpierre M, Halpern M (1971) Edades rubidio-estroncio en rocas cristalinas del sur de la República Oriental del Uruguay. Rev Asoc Geol Arg 25:138–151

Wasserburg G (1963) Diffusion processes in lead-uranium systems. J Geophys Res 68:4823–4846

Wetherill G (1956) Discordant uranium-lead ages I. Am Geophys U Trans 37:320–326

Williams IS (1998) U-Th-Pb geochronology by ion microprobe. In: McKibben MA, Shanks III WC, Ridley WI (eds) Applications of microanalytical techniques to understanding mineralising processes. Soc Eco Geo (Rev Eco Geol) vol 7: pp 1–35